AFM Study on Protein Immobilization on Charged Surfaces at the Nanoscale: Toward the Fabrication of Three-Dimensional Protein Nanostructures

ARTICLE *in* LANGMUIR · NOVEMBER 2003

Impact Factor: 4.46 · DOI: 10.1021/la035491q

AFM Study on Protein Immobilization on Charged Surfaces at the Nanoscale: Toward the Fabrication of Three-Dimensional Protein Nanostructures

Dejian Zhou, Xiuzhu Wang, Louise Birch, Trevor Rayment, and Chris Abell*

Department of Chemistry, University of Cambridge, Lensfield Road, Cambridge CB2 1EW, United Kingdom

Received August 14, 2003. In Final Form: September 23, 2003

Three differently charged nanoscale features were constructed by sequential nanografting of 6-mercaptohexan-1-ol, *N*-(6-mercapto)hexylpyridinium bromide, and 3-mercaptopropionic acid into a self-assembled monolayer resist of an alkanethiol terminated with a hexa(ethylene glycol) group on an atomically flat template stripped gold surface. The immobilization of three proteins, lysozyme, rabbit IgG, and bovine carbonic anhydrase (II), onto these different charged nanopatches was studied at a variety of pH values. At pH 4.5, all three proteins adsorbed onto the charged nanosurfaces. At higher pH, the proteins behaved differently, depending on the pH and relative surface charge of the nanosurface. A surface charge distribution model was employed to explain the unusual adsorption behavior of carbonic anhydrase. Finally, an approach that combines electrostatic immobilization and specific protein−protein interactions to fabricate multiple-layered (protein G/rabbit IgG/anti-IgG) three-dimensional (3D) protein nanostructures is presented, demonstrating that the combination of nanografting, electrostatic immobilization, and specific protein interaction is a powerful tool for construction of novel 3D protein surface nanostructures.

Introduction

The immobilization of proteins onto a defined position of a surface while still maintaining their biological functionality is of crucial importance to some array-based screening techniques.[1−4] Three main types of surface attachment techniques have been used to immobilize proteins onto surfaces: physical adsorption (including electrostatic and hydrophobic interactions),[5−12] covalent attachment (e.g., through gold−thiol interactions, amide or imine bond formation, silane chemistry, etc.),[8,13,14] and biospecific interactions (e.g., exploiting biotin−streptavidin, antibody−antigen, DNA hybridizations, etc.).[15,16]

The use of electrostatic interactions is an attractive route for attaching proteins onto solid surfaces due to its practical simplicity. Such interactions are usually reversible yet relatively robust and, most importantly, can maintain the biological functionality of the immobilized proteins.[7,17−19] This approach has been used to attach protein molecules onto nanostructured metal oxide surfaces to make optical and electrochemical biosensors.[7,17] It is generally believed that the overall charge of the protein molecules is responsible for their attachments onto oppositely charged surfaces,[8] although contrary examples have also been reported.[7]

In this paper, we describe a model system to systematically study protein immobilization on electrically charged surfaces at the nanoscale. We have used a self-assembled monolayer (SAM) of an alkanethiol terminated with a hexa(ethylene glycol) ($(EG)_6$) group, which is known to resist nonspecific adsorption of protein molecules as a resist layer,[20−26] into which a series of differently charged nanopatches were constructed by sequentially nanograft-

* To whom correspondence should be addressed. Tel: +44-1223-336405. Fax: +44-1223-336362. E-mail: ca26@cam.ac.uk.

(1) MacBeath, G.; Schreiber, S. L. *Science* **2000**, *289*, 1760−1763.
(2) Niemeyer, C. M.; Blohm, D. *Angew. Chem., Int. Ed.* **1999**, *38*, 2865−2869.
(3) Wilson, D. S.; Nock, S. *Angew. Chem., Int. Ed.* **2003**, *42*, 494−500.
(4) Wilson, D. S.; Nock, S. *Curr. Opin. Chem. Biol.* **2002**, *6*, 81−85.
(5) Liu, G. Y.; Amro, N. A. *Proc. Natl. Acad. Sci. U.S.A.* **2002**, *99*, 5165−5170.
(6) Michel, B.; Bernard, A.; Bietsch, A.; Delamarche, E.; Geissler, M.; Juncker, D.; Kind, H.; Renault, J. P.; Rothuizen, H.; Schmid, H.; Schmidt-Winkel, P.; Stutz, R.; Wolf, H. *IBM J. Res. Dev.* **2001**, *45*, 697−719.
(7) Topoglidis, E.; Campbell, C. J.; Cass, A. E. G.; Durrant, J. R. *Langmuir* **2001**, *17*, 7899−7906.
(8) Wadu-Mesthrige, K.; Amro, N. A.; Garno, J. C.; Xu, S.; Liu, G. Y. *Biophys. J.* **2001**, *80*, 1891−1899.
(9) Inerowicz, H. D.; Howell, S.; Regnier, F. E.; Reifenberger, R. *Langmuir* **2002**, *18*, 5263−5268.
(10) Renault, J. P.; Bernard, A.; Bietsch, A.; Michel, B.; Bosshard, H. R.; Delamarche, E.; Kreiter, M.; Hecht, B.; Wild, U. P. *J. Phys. Chem. B* **2003**, *107*, 703−711.
(11) Renault, J. P.; Bernard, A.; Juncker, D.; Michel, B.; Bosshard, H. R.; Delamarche, E. *Angew. Chem., Int. Ed.* **2002**, *41*, 2320−2323.
(12) (a) Bruckbauer, A.; Ying, L. M.; Rothery, A. M.; Zhou, D. J.; Shevchuk, A. I.; Abell, C.; Korchev, Y. E.; Klenerman, D. *J. Am. Chem. Soc.* **2002**, *124*, 8810−8811. (b) Bruckbauer, A.; Zhou, D. J.; Ying, L. M.; Korchev, Y. E.; Abell, C.; Klenerman, D. *J. Am. Chem. Soc.* **2003**, *125*, 9834−9839.
(13) Kenseth, J. R.; Harnisch, J. A.; Jones, V. W.; Porter, M. D. *Langmuir* **2001**, *17*, 4105−4112.
(14) Wilson, D. L.; Martin, R.; Hong, S.; Cronin-Golomb, M.; Mirkin, C. A.; Kaplan, D. L. *Proc. Natl. Acad. Sci. U.S.A.* **2001**, *98*, 13660−13664.
(15) Whitesides, G. M.; Ostuni, E.; Takayama, S.; Jiang, X. Y.; Ingber, D. E. *Annu. Rev. Biomed. Eng.* **2001**, *3*, 335−373.
(16) Kane, R. S.; Takayama, S.; Ostuni, E.; Ingber, D. E.; Whitesides, G. M. *Biomaterials* **1999**, *20*, 2363−2376.
(17) Topoglidis, E.; Cass, A. E. G.; O'Regan, B.; Durrant, J. R. *J. Electroanal. Chem.* **2001**, *517*, 20−27.
(18) Lee, K. B.; Park, S. J.; Mirkin, C. A.; Smith, J. C.; Mrksich, M. *Science* **2002**, *295*, 1702−1705.
(19) Ladam, G.; Schaaf, P.; Cuisinier, F. J. G.; Decher, G.; Voegel, J. C. *Langmuir* **2001**, *17*, 878−882.
(20) Prime, K. L.; Whitesides, G. M. *Science* **1991**, *252*, 1164−1167.
(21) Prime, K. L.; Whitesides, G. M. *J. Am. Chem. Soc.* **1993**, *115*, 10714−10721.
(22) Palegrosdemange, C.; Simon, E. S.; Prime, K. L.; Whitesides, G. M. *J. Am. Chem. Soc.* **1991**, *113*, 12−20.
(23) Schwendel, D.; Dahint, R.; Herrwerth, S.; Schloerholz, M.; Eck, W.; Grunze, M. *Langmuir* **2001**, *17*, 5717−5720.
(24) Sharma, S.; Popat, K. C.; Desai, T. A. *Langmuir* **2002**, *18*, 8728−8731.
(25) (a) Jang, C. H.; Stevens, B. D.; Carlier, P. R.; Calter, M. A.; Ducker, W. A. *J. Am. Chem. Soc.* **2002**, *124*, 12114−12115. (b) Jang, C. H.; Stevens, B. D.; Philips, R.; Calter, M. A.; Ducker, W. A. *Nano Lett.* **2003**, *3*, 691−694.
(26) Veiseh, M.; Zareie, M. H.; Zhang, M. Q. *Langmuir* **2002**, *18*, 6671−6678.

10.1021/la035491q CCC: $25.00
Published on Web 11/07/2003

ing[5,27,28] the charged alkanethiols into the SAM. To facilitate the visualization of the topographic change, ultraflat template stripped gold (TSG) surfaces[29,30] were used to prepare the SAMs. The adsorption of different proteins onto these charged patches at a variety of pH values was studied by atomic force microscopy (AFM). Our results demonstrate that AFM is a powerful tool to create multifunctionalized surfaces at the nanoscale. We show that protein immobilization on charged surfaces is not simply due to the overall charge of the protein relative to that of the surface, but is rather more complicated, and that surface charge of localized protein domains may also play an important role.

Layer-by-layer assembly, which mainly uses the electrostatic attractions between oppositely charged polymers, has been used to fabricate multilayered films and microscale structures of charged synthetic polymers.[31−33] Similarly, proteins can also be used as building blocks to assemble novel nanostructures[15,34] and to build up multilayered protein films on surfaces.[35] The use of charged nanosurfaces created in a SAM that resists adsorption of proteins should allow us to position proteins and build up protein nanofeatures on surfaces.[5,8,27] In this paper, we have explored this possibility through the use of a SAM of an alkanethiol terminated with an EG_6 group as the protein-adsorption-resisting coating into which charged nanostructures were introduced through nanografting.[27] The nanostructured surface was used as the template to assemble the multilayered (protein G/IgG/anti-IgG) protein nanostructures through electrostatic immobilization and the biospecific antibody−antigen interactions. The whole fabrication process was monitored by AFM in situ.

Experimental Section

Materials. All materials and reagents, HPLC-grade ethanol, 1,6-dibromohexane (98%), potassium thiolacetate (99%), anhydrous pyridine (99.5%), hydrobromic acid, 6-mercaptohexan-1-ol (MCH, 97%), 3-mercaptopropionic acid (MPA, 98%), lysozyme (95%) from chicken egg white, rabbit immunoglobulin G (IgG, 95%), goat anti-rabbit IgG, protein G, and carbonic anhydrase isozyme II from bovine erythrocytes were purchased from Sigma-Aldrich Co. (Dorset, U.K.) and used as received. Ultrapure MilliQ water (resistance > 18 MΩ.cm) was used for all the buffer solutions and for rinsing sample surfaces. Unless otherwise stated, "water" means MilliQ water. PBS buffer was used for near neutral and higher pH solutions (10 mM phosphate, 150 mM NaCl, 2 mM NaN_3, pH 7.2 and pH 11.5). Sodium acetate buffer was used for low pH solutions (20 mM sodium acetate, 100 mM NaCl, pH values were 4.5, 5.0, and 5.5). The protein concentrations used in this study were all 0.10 mg/mL unless otherwise stated. All the buffered solutions were filtered through a Whatman syringe filter (0.20 μm pore size, Whatman Plc., U.S.).

Synthesis. 11-Mercaptoundecyl hexa(ethylene glycol) alcohol ($C_{11}(EG)_6$) was synthesized by following a literature method.[21,22] The compound was purified by flash column chromatography on silica gel (10% ethanol in ethyl acetate) as a colorless oil. ^{1}H NMR (400 MHz, $CDCl_3$, δ ppm): 1.20−1.37 (m, 14H, 7CH_2), 1.49−1.60 (m, 4H, 2CH_2), 2.47 (q, 2H, J = 7.0 Hz, HSCH_2−), 2.70 (s, br, 1H, −O*H*), 3.39 (t, 2H, J = 7.0 Hz, −CH_2EG), 3.50−3.70 (m, 24H, 6*EG*). ^{13}C NMR (100 MHz, $CDCl_3$, δ ppm): 72.3, 71.3, 70.3, 70.1, 69.8, 61.5, 33.8, 29.4, 29.3, 29.2, 29.0, 28.8, 28.1, 25.8, 24.4 (several peaks are overlapping in the ^{13}C NMR spectrum). HRMS (Q-TOF): found, 533.3118; required for $C_{25}H_{50}O_8SNa$ [M + Na]$^+$, 533.3124.

Scheme 1. Synthetic Route to MHP.Br

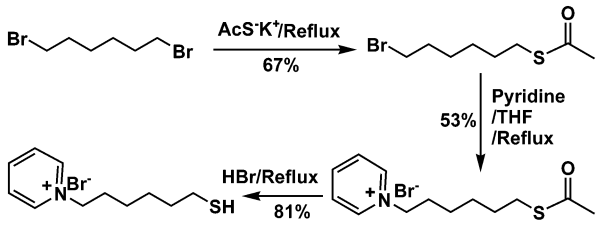

Scheme 1 shows the synthetic route to the positively charged thiol (*N*-(6-mercaptohexyl) pyridinium bromide). At first, 1,6-dibromohexane was converted to the monothiolacetate by reaction of potassium thiolacetate with 1,6-dibromohexane. The major side product from this reaction was the bisthiolacetate. The occurrence of this product was reduced by using an excess of 1,6-dibromohexane, leading to a yield of 67% for the monothiolacetate. This was then converted to the corresponding pyridinium salt by reaction with excess pyridine. Finally, the pyridinium thiol (MHP.Br) was obtained by deprotection of the thiolacetate using acidic hydrolysis.[21,22] To avoid the need for anion exchange, HBr was used instead of HCl. The detailed synthetic procedures are described below.

Synthesis of 6-Bromohexylthiolacetate. To a 150 mL dry tetrahydrofuran (THF) solution containing 19.3 g of 1,6-dibromohexane (79.2 mmol) was added 4.52 g of potassium thiolacetate (39.6 mmol), and the resulting suspension was heated at reflux with stirring for 24 h under N_2. After cooling to room temperature, the suspension was filtered and the residue was washed with 20 mL of THF. The combined THF solution was evaporated to dryness to obtain a yellowish oil, which was purified on a silica gel column using 2:1 (v/v) hexane/dichloromethane (DCM) as the eluant to give the acetate (6.33 g, 67%) as a colorless oil. R_f: 0.31 (2:1 v/v hexane/DCM). ^{1}H NMR (400 MHz, $CDCl_3$, δ ppm): 3.38 (2H, t, J = 7.2 Hz, Br−CH_2−), 2.84 (2H, t, J = 7.2 Hz, AcSCH_2−), 2.30 (3H, s, CH_3(C═O)−), 1.83 (2H, qn, J = 7.2 Hz, BrCH$_2$CH_2−), 1.57 (2H, qn, J = 7.2 Hz, AcSCH$_2$CH_2−), 1.31−1.48 (4H, m, 2CH_2). ^{13}C NMR (100 MHz, $CDCl_3$, δ ppm): 195.3 (*C*═O), 33.1, 32.0, 30.1, 28.8, 28.8 27.3, 27.1

Synthesis of N-(6-Acetylthiolhexyl) Pyridinium Bromide. To 6-bromohexylthiolacetate (1.42 g, 5.94 mmol) in 20 mL of THF was added pyridine (1.96 g, 24.8 mmol). The resulting solution was heated at reflux for 3 days. The solvent and unreacted pyridine were removed under reduced pressure. The residue was washed with diethyl ether (2 × 10 mL) and hexane (1 × 10 mL) and dried in vacuo to obtain a yellow oil, which was then dissolved in acetone (5 mL) and subsequently precipitated by the addition of diethyl ether (20 mL) to give the bromide (0.97 g, 53%) as a white solid. ^{1}H NMR (400 MHz, $CDCl_3$, δ ppm): 9.55 (2H, d, J = 7.1 Hz, 2*H*−Py$^+$), 8.52 (1H, m, *H*−Py$^+$), 8.12 (2H, t, J = 7.1 Hz, 2*H*−Py$^+$), 4.99 (2H, t, J = 7.5 Hz, CH_2−Py$^+$), 2.77 (2H, t, J = 7.2 Hz, AcSCH_2−), 2.26 (3H, s, CH_3(C═O)−), 1.98−2.07 (2H, m, CH_2), 1.45−1.54 (2H, m, CH_2), 1.33−1.43 (4H, m, 2CH_2). ^{13}C NMR (100 MHz, $CDCl_3$, δ ppm): 197.7 (*C*═O), 145.6 (*C*−Py$^+$), 145.5 (2*C*−Py$^+$), 128.8 (2*C*−Py$^+$), 62.2 (*C*H$_2$Py$^+$), 32.2, 31.1, 29.5, 29.1, 28.3, 25.8.

Synthesis of N-(6-Mercaptohexyl) Pyridinium Bromide (MHP.Br). *N*-(6-Acetylthiolhexyl) pyridinium bromide (0.97 g, 3.05 mmol) was dissolved in HBr (20 mL, 1 M) in a mixed solution of MeOH and H_2O (50/50 v/v), which was heated at reflux under N_2 for 12 h. The solvents were removed under reduced pressure, and the residue was purified by column chromatography on silica gel using 10% MeOH in DCM as the eluent. The bromide (0.68 g, 81%) was obtained as a white solid. ^{1}H NMR (400 MHz, CD_3OD, δ ppm): 9.22 (2H, d, J = 7.1 Hz, 2*H*−Py$^+$), 8.69 (1H, m, H−Py$^+$), 8.19 (2H, t, J = 7.1 Hz, 2*H*−Py$^+$), 4.78 (2H, t, J = 7.4 Hz, CH_2−Py$^+$), 2.46 (2H, t, J = 7.2 Hz, HSCH_2−), 2.06 (2H, m, CH_2), 1.52−1.61 (2H, m, CH_2), 1.35−1.51 (4H, m, 2CH_2). ^{13}C NMR (100 MHz,

(27) Liu, G. Y.; Xu, S.; Qian, Y. L. *Acc. Chem. Res.* **2000**, *33*, 457−466.
(28) Xu, S.; Laibinis, P. E.; Liu, G. Y. *J. Am. Chem. Soc.* **1998**, *120*, 9356−9361.
(29) Hegner, M.; Wagner, P.; Semenza, G. *Surf. Sci.* **1993**, *291*, 39−46.
(30) Wagner, P.; Hegner, M.; Guntherodt, H. J.; Semenza, G. *Langmuir* **1995**, *11*, 3867−3875.
(31) Decher, G. *Science* **1997**, *277*, 1232−1237.
(32) Shi, F.; Dong, B.; Qiu, D. L.; Sun, J. Q.; Wu, T.; Zhang, X. *Adv. Mater.* **2002**, *14*, 805−809.
(33) Vazquez, E.; Dewitt, D. M.; Hammond, P. T.; Lynn, D. M. *J. Am. Chem. Soc.* **2002**, *124*, 13992−13993.
(34) Niemeyer, C. M. *Angew. Chem., Int. Ed.* **2001**, *40*, 4128−4158.
(35) Vijayendran, R. A.; Leckband, D. E. *Anal. Chem.* **2001**, *73*, 471−480.

CD_3OD, δ ppm): 147.5 ($C-Py^+$), 146.6 ($2C-Py^+$), 130.1 ($2C-Py^+$), 63.4 (CH_2Py_+), 35.2, 33.0, 29.1, 27.0, 25.5.

Template Stripped Gold.[29,30] Gold (>99.99%) was thermally evaporated onto freshly cleaved mica surfaces prebaked at 300 °C overnight at a rate of 0.1 nm/s to a thickness of 150−200 nm under a base pressure of 6×10^{-7} Torr. The gold-coated mica sheet was then annealed at 300 °C for 8 h in the evaporator chamber before being taken out and cut into 1.2×1.2 cm^2 pieces. They were glued to cleaned silicon pieces with the gold face down using Epo Tek 377 glue. The silicon/glue/gold/mica sandwiches were baked in an oven at 150 °C for 2 h. TSG surfaces were obtained by using the chemical stripping method with THF.[29,30] After stripping, the surfaces were washed with ethanol and water and dried under a stream of nitrogen. The freshly prepared TSG surfaces were extremely flat, with a typical surface roughness of less than 3 Å over a surface area of 25 μm^2.[36] Once stripped, the TSG surfaces were used immediately to avoid contamination. Typically, a SAM of the $C_{11}(EG)_6$ thiol was prepared by incubating a TSG surface with a 2 mM $C_{11}(EG)_6$ thiol solution in ethanol overnight, rinsed with ethanol, and dried over a stream of N_2.

Ellipsometry Measurements. The thickness of the SAMs on TSG was measured on an EL X-02C ellipsometer (DRE, Germany) at an incident angle of 70° using a He−Ne laser at 632.8 nm.[37] The refractive indices of the TSG substrates were first measured and calculated with a two-phase parallel-layer model (gold/air) from classical electromagnetic theory. SAMs of the thiols were prepared by incubation of freshly cleaved TSG surfaces with a 2 mM ethanol (for $C_{11}(EG)_6$) or aqueous solution of the corresponding thiols for 24 h, rinsed thoroughly with ethanol and water, and dried over a stream of N_2. After SAM formation, at least six different spots on each of two samples for each SAM layer were analyzed, and the thickness of the organic film was determined from a three-phase model (gold/organic/air) and averaged. A real refractive index of 1.50 (the imaginary refractive index part is zero as the samples are transparent at 632.8 nm) for the organic film and the previously measured refractive indexes for the TSG substrate were used to evaluate the film thickness.[37,38]

Atomic Force Microscopy. All of the AFM experiments were carried out on a Digital Instruments (Veeco, Santa Barbara, CA) Dimension 3100 AFM with a Nanoscope IV controller. All the images were collected with a custom-made fluid cell under water or a buffer solution at 24 ± 1 °C. Standard oxidized sharpened V-shaped Si_3N_4 microlevers from Digital Instruments with a nominal spring constant of 0.32 or 0.58 N/m were used in all image collections and nanografting experiments. Images were collected at a scan rate of 2 Hz and at a scan angle of 90°. The captured images were analyzed with the Nanoscope image analyzing software using first-order flattening.[36,37]

The nanografting followed a literature procedure.[5,27,36] A sample of the $C_{11}(EG)_6$ SAM on TSG was imaged under a low loading force (typically in the range of 0.5−1 nN) under an aqueous solution of the thiol (2 mM) which was to be nanografted into the SAM, that is, MHP.Br, MPA, or MCH. A suitable small area (usually 400×400 nm^2 or 200×200 nm^2) was then selected for nanografting. The area was repeatedly scanned under a high loading force (i.e., 100−150 nN) by increasing the deflection set point voltage by several units to scrape away the $C_{11}(EG)_6$ SAM resist.[13,36] During the scan, the thiol molecules in the solution filled the freshly exposed gold surface by self-assembly to form a SAM terminating with the desired surface charge properties.[27,28] Nanografting was conducted at a scan rate of 4−5 Hz, and typically 3−5 scans were applied to completely replace the $C_{11}(EG)_6$ SAM with the desired thiol. After nanografting, the AFM tip was completely withdrawn from the surface by decreasing the deflection setpoint. The scan rate was changed to 2 Hz, and the scan area was increased. Then the tip was re-engaged with the minimum loading force to take topographic images. After each manipulation, the remaining solution was removed from the fluid cell, the surface was thoroughly washed with MilliQ water, followed by the same buffer to be used in the next step, and then the desired new solution was introduced and incubated.

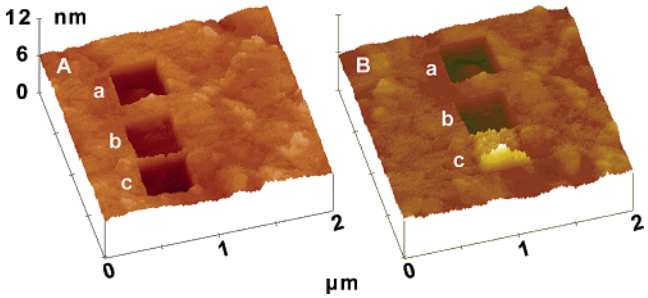

Figure 1. AFM 3D topographic images. (A) Three differently charged nanopatches (400×400 nm^2 each) created by nanografting of MCH (neutral hydrophilic (a)), MHP (positive (b)), and MPA (negative (c)) into the SAM of $C_{11}(EG)_6$. (B) After incubation of the sample in image A with lysozyme (0.10 mg/mL in PBS, pH 7.20) for 20 min, only the MPA hole was filled. Both images are in the same scan size (2×2 μm^2) and z-scale.

Surface Charge Modeling of Carbonic Anhydrase. Electrostatic surfaces at each pH state were produced using WebLab ViewerPro (Accelrys Inc., San Diego, CA; WebLab ViewerPro, v4.0, 2000) and colored according to the electrostatic potential. The crystal structure for bovine carbonic anhydrase II downloaded from the protein data bank (PDB, PDB code 1a42) was used for the modeling.[39,40] The ligand and all crystallographic water molecules were removed from the structure, and hydrogen atoms were theoretically added to each amino acid residue using Insight II (Accelrys Inc., San Diego, CA; Insight II, v2000, 2000) depending on the pH. The environmental pH was allowed to increase from 3.0 to 10.0 in half pH unit increments, and the protonation states of ionizable residues were set to those tabulated by Insight II.

Results and Discussion

Determination of SAM Thickness by Ellipsometry.[37] SAMs of $C_{11}(EG)_6$, MHP, MCH, and MPA on TSG were prepared, and their thicknesses were found to be 3.0 ± 0.3, 1.2 ± 0.3, 1.0 ± 0.3, and 0.5 ± 0.2 nm, respectively. These values are in good agreement with the literature values.[22]

Construction of Multiple Differently Charged Nanopatches on a Single Surface through Sequential Nanografting. Following the pioneering work of Liu et al., the use of nanografting to generate nanoscale surfaces with desired functionality has been reported by several groups.[5,13,25,27,36,37,41,42] In principle, combining relatively stable SAMs of alkanethiols on gold with sequential nanografting should make it possible to construct multiple nanoscale surfaces with different functionalities on a single surface.[25b] In this study, by sequential nanografting of MCH, MHP, and MPA into different locations of the $C_{11}EG_6$ SAM, we have constructed three differently charged nanosquares, positive (MHP), neutral (MCH), and negative (MPA), on the same surface (Figure 1A). To minimize the possible thiol exchange between the thiols previously self-assembled within a nanosquare and those in solution during the next nanografting, sequential nanografting was carried out in the

(36) (a) Zhou, D. J.; Sinniah, K.; Abell, C.; Rayment, T. *Langmuir* **2002**, *18*, 8278−8281. (b) Zhou, D. J.; Sinniah, K.; Abell, C.; Rayment, T. *Angew. Chem., Int. Ed.* **2003**, *42*, 4934−4937.

(37) Wang, X. Z.; Zhou, D. J.; Rayment, T.; Abell, C. *Chem. Commun.* **2003**, 474−475.

(38) Bain, C. D.; Troughton, E. B.; Tao, Y. T.; Evall, J.; Whitesides, G. M.; Nuzzo, R. G. *J. Am. Chem. Soc.* **1989**, *111*, 321−335.

(39) Berman, H. M.; Westbrook, J.; Feng, Z.; Gilliland, G.; Bhat, T. N.; Weissig, H.; Shindyalov, I. N.; Bourne, P. E. *Nucleic Acids Res.* **2000**, *28*, 235−242.

(40) Stams, T.; Chen, Y.; Boriack-Sjodin, P. A.; Hurt, J. D.; Liao, J.; May, J. A.; Dean, T.; Laipis, P.; Silverman, D. N.; Christianson, D. W. *Protein Sci.* **1998**, *7*, 556−563.

(41) Liu, J. F.; Cruchon-Dupeyrat, S.; Garno, J. C.; Frommer, J.; Liu, G. Y. *Nano Lett.* **2002**, *2*, 937−940.

(42) Liu, M. Z.; Amro, N. A.; Chow, C. S.; Liu, G. Y. *Nano Lett.* **2002**, *2*, 863−867.

order of their relative stability, that is, MCH first, then MHP, and finally MPA. The average depths of the MCH, MHP, and MPA nanopatches are 1.9 ± 0.3, 1.8 ± 0.3, and 2.4 ± 0.3 nm, respectively. The depths of the holes are in very good agreement with the SAM thickness differences measured by ellipsometry between the $C_{11}(EG)_6$ SAM and those of the three nanografted thiols, suggesting that the sequential nanografting operation was successful. Once prepared, the depth of the nanografted nanoholes did not change throughout the whole nanografting procedure, suggesting there is no detectable thiol exchange and nonspecific adsorption of undesired contaminants.

Immobilization of Lysozyme onto Charged Nanopatches. The immobilization of protein molecules onto charged nanopatches created by nanografting has been reported.[5,8,13,27] However, in most cases, the matrix surface coating (SAM resist layer) was a simple alkanethiol, which may cause problems due to nonspecific adsorption, and surfactant washing proved necessary.[8,27] In this study, the SAM of an alkanethiol terminating with a EG_6 group was used, which significantly reduced the undesired nonspecific adsorption of proteins.[13,20,21,25]

After incubating the surface shown in Figure 1A with a lysozyme solution in PBS buffer (pH 7.2) for 10 min, the topography of the nanoholes had already changed (Figure 1B). It is clear that the lysozyme molecules exclusively attach to the MPA patch to form a complete protein layer, which protrudes by 1.0 nm above the surrounding $C_{11}EG_6$ matrix, while the MHP and MCH nanopatches remain uncovered. The average thickness of the protein layer was 3.4 nm, taking into account the original hole depth. Line scan profiles reveal that the protein molecules within the patch protrude by 0.5−2.5 nm above the $C_{11}EG_6$ matrix. As lysozyme is ellipsoidal, with approximate dimensions of $4.5 \times 3.0 \times 3.0$ nm^3,[8,46] our data suggest it adopts a variety of orientations within the nanopatch. Similar results have been observed by Liu et al.[8] Lysozyme has a pI of 11.1[8] and so is positively charged at pH 7.2. The pK_a of the MPA SAM is 7.7,[43] so around 25% of the carboxylic acid groups within the grafted nanopatch would be deprotonated. This suggests the interaction was mainly electrostatic.[8] When the same experiment was carried out at pH 11.5 (in PBS buffer), so that the protein would be slightly negatively charged, none of the three nanopatches were found to be filled with lysozyme, that is, there was no difference in the depths of the holes before and after the protein incubation. After removing the lysozyme solution (pH 11.5) followed by thorough washing of the surface with the PBS buffer (pH 7.2), it was found that reintroduction of lysozyme solution (pH 7.2) for 10 min caused only the negatively charged MPA nanopatch to be covered with a layer of lysozyme. The MHP and MCH patches remained uncovered. This suggests that nanopatches created by sequential nanografting are stable at the relatively high pH of 11.5 with no detectable thiol exchanges during the sequential nanografting procedure.

In contrast, at pH 4.5 (in acetate buffer, where the protein would be positively charged), it was found that lysozyme immobilized onto both the MPA and the positive MHP nanopatches. These observations suggest that the overall charge of the lysozyme molecules is not the only factor that determines surface immobilization. Lysozyme did not immobilize onto the neutral hydrophilic MCH nanopatches at the pH values studied above. The average protein layer thicknesses measured in the different experiments are summarized in Table 1.

Table 1. Average Protein Layer Thickness (nm) of Lysozyme and Rabbit IgG Immobilized onto the Positively Charged MHP, Negatively Charged MPA, and Neutral MCH Nanopatches at Different pHs

	pH		
surface	4.5	7.2	11.5
lysozyme/MHP	3.0 ± 0.8	~0	~0
lysozyme/MHP	2.7 ± 0.5	3.5 ± 0.5	~0
lysozyme/MCH	~0	~0	~0
IgG/MHP	4.5 ± 1.0	5.7 ± 1.0	*a*
IgG/MPA	4.5 ± 1.0	6.0 ± 1.0	*a*
IgG/MCH	0.3 ± 0.3	0.3 ± 0.3	*a*

[a] Not determined, primarily because the pH is too high relative to the pI.

As shown in Table 1, when the same experiments were carried out with rabbit IgG, it was found that the IgG molecules immobilized onto both the negatively and positively charged nanopatches at both pH 7.2 and 4.5, forming a complete protein layer. A similar thickness has also been reported for IgG immobilized on negatively charged nanopatches and by covalent attachment.[5,8] The immobilized IgG molecules appeared to have maintained their biological functionality since when the samples were incubated with goat anti-rabbit IgG for 20 min in PBS buffer (pH 7.2), the height of the IgG nanopatches increased by ca. 8 nm, suggesting a specific antigen−antibody interaction. As in the case of lysozyme, little adsorption onto the MCH patch was observed at pH 7.2 and 4.5 (a few scattered IgG molecules were found to be loosely adsorbed on the MCH patch; however, they were readily removed by the AFM tip during the image scan). The pIs of IgGs range from 5 to 7, so it is expected that the overall protein net charge would be slightly negative at pH 7.2 and positive at pH 4.5.

Carbonic anhydrase II (CA) is a monomeric globular zinc metalloenzyme of molecular weight 29 kDa which catalyzes the hydration of carbon dioxide to form carbonic acid.[44] The enzyme has a pI of 5.9. The attachment of CA onto solid surfaces and its binding interaction with a variety of inhibitors have been studied by surface plasmon resonance (SPR)[45−47] and by force spectroscopy.[48] However, it was found that significant numbers of CA molecules are immobilized onto the dextran surface only at relatively low pH (≤5.0) through EDC−NHS coupling.[45,46,48] When the immobilization was carried out at pH 7.4, only a small fraction of an enzyme monolayer was found to attach to the surface.[45,48] To understand this, a detailed study on the pH dependence on the immobilization of CA at the charged surfaces was carried out. Representative AFM topographic images of the CA immobilized onto the positively charged MHP nanopatches created by nanografting at pH 4.5, 5.0, and 5.5 are shown in Figure 2. Table 2 summarizes the details of CA layer thickness measured by AFM at the different pHs at the charged nanosurfaces.

At pH 4.5, CA was found to be immobilized onto both the negatively and positively charged patches to form a protein layer of 7−8 nm thick, which roughly corresponds

(43) Hu, K.; Bard, A. J. *Langmuir* **1997**, *13*, 5114−5119.

(44) Christianson, D. W.; Fierke, C. A. *Acc. Chem. Res.* **1996**, *29*, 331−339.

(45) Lahiri, J.; Isaacs, L.; Tien, J.; Whitesides, G. M. *Anal. Chem.* **1999**, *71*, 777−790.

(46) Svedhem, S.; Enander, K.; Karlsson, M.; Sjobom, H.; Liedberg, B.; Lofas, S.; Martensson, L. G.; Sjostrand, S. E.; Svensson, S.; Carlsson, U.; Lundstrom, I. *Anal. Biochem.* **2001**, *296*, 188−196.

(47) Ostuni, E.; Grzybowski, B. A.; Mrksich, M.; Roberts, C. S.; Whitesides, G. M. *Langmuir* **2003**, *19*, 1861−1872.

(48) Sinniah, K.; Wang, X. Z.; Zhou, D. J.; Abell, C.; Rayment, T. *Abstr. Pap. Am. Chem. Soc.* **2002**, *224*, 032-COLL.

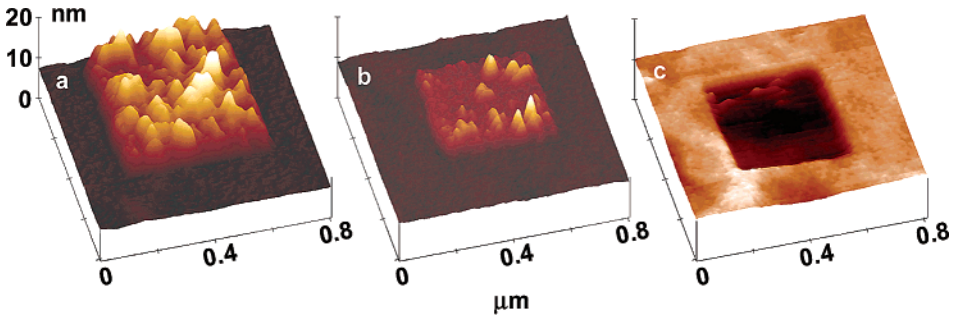

Figure 2. Representative AFM 3D topographic images showing the immobilization of carbonic anhydrase onto the positively charged MHP nanopatch at pH 4.5 (a), 5.0 (b), and 5.5 (c). All images have the same scan size (800 × 800 nm^2) and *z*-scale.

Table 2. Average Protein Layer Thickness (nm) of Carbonic Anhydrase Immobilized onto the Positively Charged MHP, Neutral MCH, and Negatively Charged MPA Nanopatches at Different pH Values

	pH			
surface	4.5	5.0	5.5	7.2
MHP	8.1 ± 0.6	4.4 ± 0.2	0.1 ± 0.1	0.3 ± 0.2
MHP	7.4 ± 0.6	4.0 ± 0.2	3.9 ± 0.2	4.0 ± 0.2
MCH	∼0	∼0	∼0	∼0

to a double layer of CA (CA has a diameter of approximately 4.0 nm).[45] A careful analysis of line scan profiles of the CA nanopatch at pH 4.5 reveals that the protein layer is not uniform, with the main part of the protein layer to be around 4−5 nm thick with domains up to 13 nm high (∼3 protein layers) (Figure 3), suggesting that some CA molecules have aggregated at this pH. Interestingly, the protein adsorbed very quickly onto the charged surfaces (≤10 min from a 0.05 mg/mL solution) to reach saturation, and no significant change in the average protein layer thickness was observed over an extended incubation period of 3 h. At pH 5, the protein layer thickness decreased to ca. 4 nm (monolayer) on both negatively and positively charged surfaces. At pH 5.5 and 7.2, very little CA was immobilized onto the positively charged nanopatch, but there was still complete coverage at the negatively charged surface. At pH 5.0 and 5.5, there was much less evidence of aggregation (Figure 2b,c). Again, at all the pHs studied, there was no observable immobilization of CA onto the neutral hydrophilic MCH nanopatches.

To try to understand this adsorption behavior, the surface charge potential on CA molecules at different pHs was calculated and is shown in Figure 4. At pH 4.5, the protein molecule has a strongly positively charged domain close to the active site. There are also negatively charged domains on the protein surface even though the overall surface charge is positive. Adsorption on the negatively charged patch is expected to occur primarily through interaction with the large positively charged domain close to the active site. Immobilization of CA onto positively charged MHP nanopatches is probably due to electrostatic interactions with the smaller negatively charged domains. The domains with variable height observed for CA immobilized on the MHP nanopatch at pH 4.5 may be due to aggregation of the protein through the oppositely charged domains. Such pH-dependent aggregation may account for the higher protein attachment onto dextran surfaces at the relatively low pH (≤5.0) that has been observed previously using SPR.[45,46] At pH 6.0, the domain near the active site has lost much of its positive charge, and the overall protein is almost neutral. It is therefore surprising that there is so little adsorption onto the positively charged MHP at pH 5.5 and 7.2.

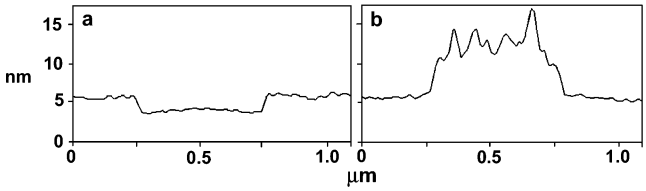

Figure 3. Representative AFM topographic line scan profiles of the MHP nanopatch created within the $C_{11}EG_6$ SAM before (a) and after (b) the immobilization of carbonic anhydrase at pH 4.5.

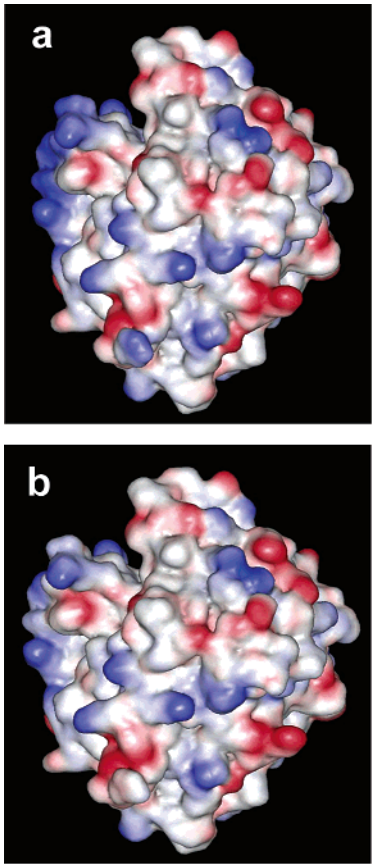

Figure 4. Electrostatic potential surfaces for bovine carbonic anhydrase II at pH 4.5 (a) and pH 6.0 (b). Regions of positive charge are shown in blue, and those of negative charge are in red.

Toward the Construction of Three-Dimensional Protein Nanostructures. The construction of uniform three-dimensional (3D) biological nanostructures is a significant challenge. Here we describe using nanografting, protein electrostatic immobilization, and specific protein−protein interactions to construct protein 3D nanostructures. The advantage of this approach rests upon

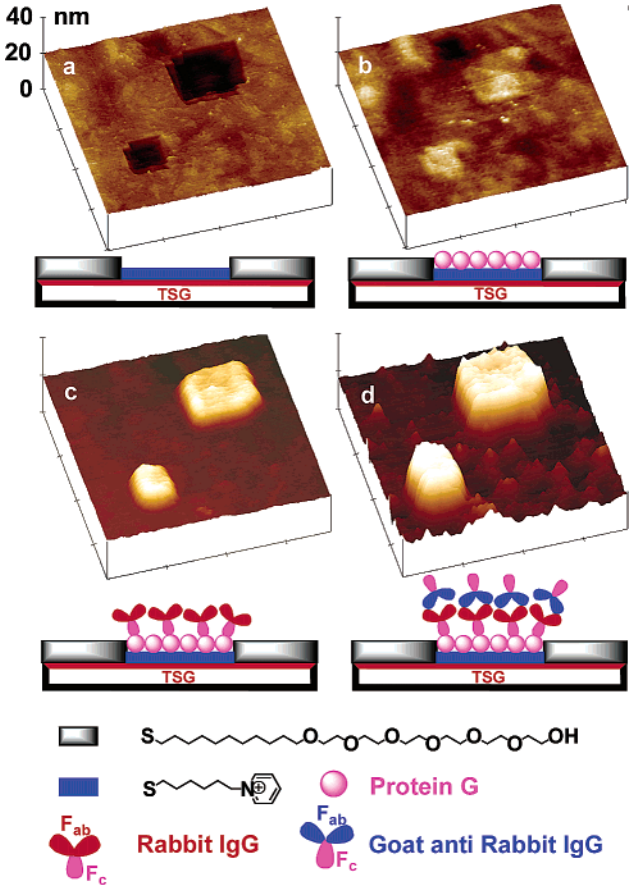

Figure 5. 3D AFM topographic images showing the process of creating and growing the 3D protein nanostructures by electrostatic immobilization and biospecific interaction. The schematics depicted underneath each image show the fabrication process of the 3D protein nanostructures. All of the images have the same scan sizes ($2 \times 2\ \mu m^2$) and have the same *z*-scale. (a) Two nanopatches (200×200 and $400 \times 400\ nm^2$) created by nanografting of MHP into the SAM of $C_{11}EG_6$ had a depth of 2 nm. The curious features in the image were the results of piezo drift during the nanografting process. (b) After incubation of the surface with protein G (0.1 mg/mL in PBS, 20 min), the patches were completely filled by protein G and transformed into plateaus with an average height of ca. 1 nm. (c) After a treatment of the surface with rabbit IgG (0.1 mg/mL in PBS, 30 min), the height of the protein nanofeatures increased to 8−9 nm. (d) After subsequent treatment of the surface with goat anti-rabbit IgG (0.1 mg/mL in PBS, 30 min), the height of the protein nanofeatures increased to 19−20 nm.

the fact that some protein molecules have multiple specific binding sites, for example, each protein G molecule has three binding sites to an IgG Fc domain, which can significantly increase the subsequent protein attachment. In addition, the whole process can be monitored by AFM in situ.

Nanografting was used to create two positively charged nanoholes within a SAM resist of $C_{11}(EG)_6$. The holes had a depth of ca. 2.0 nm, as measured from the AFM topographic image (Figure 5a). After the surface had been incubated with protein G (pH 7.2, in PBS buffer) for 20 min, the holes were transformed into plateaus protruding by ca. 1 nm above the $C_{11}(EG)_6$ SAM resist layer (Figure 5b). Thus protein G has filled the holes by 3 nm, in agreement with the dimensions of protein G molecules. Protein G has a pI of 4.5, so the protein is negatively charged at pH 7.2. The adsorption onto the positively charged MHP nanoholes was assumed to be mainly due to electrostatic interactions. Similar results have been reported where a positively charged aminosilanized glass was used to immobilize protein G onto surfaces.[12a] After further incubation of the surface with a solution of rabbit IgG for 30 min, it is clear that the original protein G nanoplateaus have significantly increased in height (Figure 5c), now protruding by ca. 9 nm above the $C_{11}(EG)_6$ SAM surface, corresponding to an additional height increase of 8 nm. Unlike the work of Liu et al., where a variety of heights (3.8−7.2 nm) were found for the immobilized IgG molecules implying a variety of different orientations,[5,27] the height increase in our protein plateaus is larger and reasonably uniform. IgG molecules are known to have dimensions of $14.5 \times 8.5 \times 4.0\ nm^3$.[50] The uniform height increase suggests that IgG molecules have adopted an edge-on configuration, with the Fc binding domain face down to bind to protein G molecules on the surface, leaving the two Fab binding points upward. Upon further exposure of the surface to a solution of goat anti-rabbit IgG antibody for 20 min, a uniform height increase of ca. 11 nm for the protein nanostructures was observed (Figure 5d). The height increase is significantly bigger than previously observed.[5,8,27] This is in accord with the idea that the binding sites of the rabbit IgG molecules are more accessible to the secondary antibody.

The use of electrostatically immobilized protein G for subsequent attachment of antibodies may prove to be a simple way of orienting antibodies on a surface, resulting in more active recognition surfaces. Higher specific activities have been reported for IgG immobilized through a protein G layer as compared to direct covalent attachment on a homogeneous surface.[35] Here we demonstrate better binding based on topographic height measurement by AFM. The growth of the protein 3D nanostructures presented here was reasonably uniform. Thus, by choosing the proper protein−protein interactions in combination with electrostatic immobilization, it is possible to grow homogeneous complex protein 3D nanostructures with controllable height with molecular precision.

Conclusion

In conclusion, we have utilized sequential nanografting to construct multifunctionalized nanoscale features on a single surface. A systematic study on the adsorption of different protein molecules onto differently charged nanopatches revealed that in addition to the overall charge, the local domain charge of the proteins may also be important in their immobilization. Nanografting, electrostatic immobilization, and specific protein interaction have been combined to make novel 3D protein nanostructures with a uniform height on a surface. This approach combines the "top-down" and the "bottom-up" nanofabrication techniques, which can be conveniently followed by AFM and can be extended to other types of biological assemblies. Furthermore, the use of electrostatically immobilized protein G to orientate IgG molecules may prove to be useful in construction of novel antibody-based sensors.

Acknowledgment. We thank Mr. Jon Lee and Matthew Bachelor for their help in the preparation of TSG and the Leverhulme Trust and the EPSRC (U.K.) for financial support.

LA035491Q

(49) Blake, C. C. F.; Koenig, D. F.; Mair, G. A.; North, A. C. T.; Philips, D. C.; Sarma, V. R. *Nature* **1965**, *206*, 757−761.
(50) Silverton, E. W.; Navia, M. A.; Davies, D. R. *Proc. Natl. Acad. Sci. U.S.A.* **1977**, *74*, 5140−5144.